








Article

Durability of Ternary Blended Concrete Incorporating Rice Husk Ash and Calcined Clay

Joseph Mwiti Marangu ^{1,2}, Meenakshi Sharma ³, Lenka Scheinherrová ⁴, Innocent Kafodya ⁵,
Victor Kiptoo Mutai ¹, Eshrar Latif ⁶, Viviana Iris Novelli ⁷, Deepankar Kumar Ashish ⁷
and Riccardo Maddalena ^{7,*}

- ¹ Department of Physical Sciences, Meru University of Science and Technology, Meru 972-60200, Kenya; jmarangu@must.ac.ke (J.M.M.); victorkiptoo.mutai@phd.unipd.it (V.K.M.)
- ² Institute of Cement and Concrete, Meru University of Science and Technology, Meru 972-60200, Kenya
- ³ Department of Civil Engineering, Indian Institute of Technology Hyderabad, Hyderabad 502284, India; meenakshi@ce.iith.ac.in
- ⁴ Department of Materials Engineering and Chemistry, Faculty of Civil Engineering, Czech Technical University in Prague, Thákurova 7, 166 29 Prague, Czech Republic; lenka.scheinherrova@fsv.cvut.cz
- ⁵ Department of Civil Engineering, Malawi University of Business and Applied Sciences, Blantyre 312225, Malawi; ikafodya@poly.ac.mw
- ⁶ Welsh School of Architecture, Cardiff University, Cardiff CF10 3NB, UK; latife@cardiff.ac.uk
- ⁷ School of Engineering, Cardiff University, Cardiff CF24 3AA, UK; novelliv@cardiff.ac.uk (V.I.N.); ashishd@cardiff.ac.uk (D.K.A.)
- * Correspondence: maddalena@cardiff.ac.uk

Abstract: Research on the combined substitution of supplementary cementitious materials (SCMs) has already demonstrated that it might be one of the few viable options to produce low-carbon concrete at scale. This paper presents an experimental investigation on the performance and durability of rice husk ash (RHA) and calcined clay (CC) in ternary blended concrete exposed to chloride attacks under wet/dry cycles. Portland cement (PC) was replaced by RHA and CC up to 50% by weight to produce low-carbon concrete. Samples were subjected to wet/dry cycles in 3.5% NaCl water, with mineralogical composition and microstructure development before and after exposure analysed by TGA-DSC, MIP, XRD, and SEM. The durability of the concrete against wet/dry cycles was investigated in terms of compressive strength, water absorption, open porosity, density, thermal conductivity, and electrical resistivity. The results showed that concrete mixes with CC and RHA up to 60% exhibited an increase of 33% in compressive strength, followed by minimal changes in water absorption. While a decrease in electrical resistivity was measured in all samples with RHA and CC, increasing the CC content to 50% resulted in improved resistance to chloride penetration. Increasing the CC content resulted in a more refined microstructure, with an overall decrease in porosity of up to 32% compared to the control series. While RHA alone did not contribute to significant improvements after wet/dry cycles, the combined substitution of RHA and CC at SCM replacement levels of 60% showed an overall improvement in hardened properties and durability. This investigation provides valuable insights into the long-term performance and strength of innovative low-carbon concrete.

Keywords: calcined clay; rice husk ash; concrete durability; wet/dry cycle



Citation: Marangu, J.M.; Sharma, M.; Scheinherrová, L.; Kafodya, I.; Mutai, V.K.; Latif, E.; Novelli, V.I.; Ashish, D.K.; Maddalena, R. Durability of Ternary Blended Concrete Incorporating Rice Husk Ash and Calcined Clay. *Buildings* **2024**, *14*, 1201. <https://doi.org/10.3390/buildings14051201>

Academic Editor: Xiaoyong Wang

Received: 26 February 2024

Revised: 11 April 2024

Accepted: 14 April 2024

Published: 24 April 2024



Copyright: © 2024 by the authors. Licensee MDPI, Basel, Switzerland. This article is an open access article distributed under the terms and conditions of the Creative Commons Attribution (CC BY) license (<https://creativecommons.org/licenses/by/4.0/>).

1. Introduction

In an endeavour to decarbonise the concrete industry, critical innovations and solutions have been triggered to design highly durable structures [1]. The rising concern over climate change has shifted the focus to the cement industry which is one of the most energy-intensive sectors responsible for producing up to 9% of worldwide greenhouse gas emissions. The substantial growth in under-developed countries has led to a massive investment in infrastructure, representing their economic development [2]. This growth directly relates to the increase in cement production that is expected to rise exponentially by

the year 2050 [3]. Continual threats from global emissions pose challenges for researchers. Meanwhile, the disposal of agro-waste and industrial waste pose both a threat and an opportunity that researchers have been exploiting [4]. Over the past years, additional binders, other than conventional fly ash, silica fume, and GGBS, have been introduced to reduce the impact of greenhouse gases on the concrete industry [5–7]. These binders are called supplementary cementitious materials (SCMs) and are used as a replacement for Portland cement (PC) to contribute to improving the fresh, mechanical, and durability properties of concrete. Agricultural residues such as palm oil fuel ash, cassava ash, bagasse ash, and rice husk ash (RHA) demonstrate significant potential for use as SCMs. Rice husk (RH) emerges as the predominant by-product in the rice milling industry, often disposed of through open-field burning, leading to the release of toxic gases and posing various human and environmental risks [8]. Each tonne of paddy rice produces approximately 200 kg of rice husk, leading to the production of 40 kg of ash on combustion. When burnt in controlled conditions, rice husk produces ash that can contain up to 90% amorphous silica depending on the sintering temperature and duration. RHA is a promising SCM due to its higher silica content and availability in many developing countries. More than 70 million tonnes of RHA is produced annually worldwide, which can be successfully used to produce concrete [9].

Owing to the presence of a high amount of reactive SiO_2 , RHA obtained through a controlled combustion process reacts with $\text{Ca}(\text{OH})_2$ in concrete to form calcium silicate hydrate (CSH) [8]. Thus, the microstructural changes due to pozzolanic reactions modify the cement paste that adds values to cement hydration consequently increasing the strength of concrete [10]. As suggested by [11], the addition of RHA to concrete densifies its microstructure, thus reducing the porosity at later ages rather than early ages. The higher alkali content of RHA increases the pH and thus accelerates the rate of cement hydration and the pozzolanic reaction. The influence of RHA on compressive strength has been reported to depend on the water–cement ratio, the curing duration, the replacement level, and the physical and chemical properties of RHA [12]. Past studies suggest that ultrafine RHA reduces water absorption through concrete as opposed to coarse RHA, which increases water absorption compared to control concrete [13]. The advantageous effects of rice husk ash (RHA) in enhancing resistance against chloride attack, sulphate attack, and the alkali–silica reaction have been observed through the partial substitution of cement at levels ranging from 10% to 20% [12,14]. While these positive outcomes are commonly associated with lower substitution levels, typically within the range of 10% to 20%, achieving much higher levels of substitution is necessary to effectively reduce the carbon footprint of cement concrete.

The simultaneous substitution of SCMs enables increased substitution levels by fostering synergistic reactions among SCMs and ordinary Portland cement. Utilising SCMs in appropriate proportions contributes to the development of a material that is economically, technically, and environmentally viable. The incorporation of calcined clays alongside limestone (LC3) and other SCMs has demonstrated advantageous effects in achieving higher strengths and enhanced durability performance, even at elevated substitution levels [15,16]. Due to higher pozzolanic activity after calcination, kaolinitic clays among the different kinds of clays are most suitable for higher substitutions. The thermal activation of calcined clays forms highly amorphous metakaolin containing silica and alumina in an active form. These active forms of silica and alumina react with portlandite and sulphate to form C-A-S-H, ettringite, and AFm phases. Metakaolin is effective in reducing the average pore size significantly, leading to reduced water absorption and improved durability performance [17].

Limited research has been conducted on the simultaneous substitution of rice husk ash (RHA) and calcined clay (CC) in concrete. Kenya consumes approximately 300,000 metric tonnes of rice annually, increasing at a rate of 12% [18]. Kaolinite has been identified as the predominant clay mineral in the soil profiles of Africa [19,20]. Therefore, the combined

substitution of RHA and CC in cement and concrete offers a potential avenue for African countries to support their anticipated growth in the built environment.

The objective of this research is to identify the influence of high amounts of regionally available RHA and CC on the microstructure and durability properties concrete, with the ultimate goal of developing sustainable construction materials for affordable housing in Africa. Ternary blends with replacement levels of cement at 50% and 60% were prepared and analysed for compressive strength, sorptivity, porosity, density, thermal conductivity, electrical resistivity, and microstructural investigations. The durability properties were investigated by subjecting the samples to chloride attacks under wet/dry cycles.

2. Materials and Methods

2.1. Materials

A commercially available ordinary Portland cement (PC) conforming to ASTM C 150 Type 1 [21] (42.5 N/mm^2) was procured from East African Portland Cement Company Ltd. (EAPCC) in Athi River, Machakos, Kenya. Rice husk, locally available in Kenya, was incinerated at $600 \text{ }^\circ\text{C}$ for 24 h using a standard fixed-bed kiln to produce the RHA. Clay, obtained from Múkûrwe'inî (Nyeri, Kenya) (0.5609° S , 37.0488° E), was calcined at $800 \text{ }^\circ\text{C}$ for one hour in a muffle furnace. Mineralogical composition obtained from X-ray diffraction showed that phases present in the clay were mostly kaolinite and quartz, and the latter was the major phase identified in the rice husk ash. The physical and chemical properties of the powder raw materials are given in Table 1. The sum of SiO_2 , Al_2O_3 , and Fe_2O_3 in the RHA and CC was found to exceed 70%. Therefore, both RHA and CC met the ASTM C618 [22] specification for use as pozzolana/SCMs. River sand was used as fine aggregates and crushed stones were used as coarse aggregates to produce concrete mixes. Figure 1 shows the particle size distribution of fine and coarse aggregates measured using sieve analysis.

Table 1. Oxide composition (%) of rice husk ash (RHA), calcined clay (CC), and Portland cement (PC) and physical properties.

Composition	Rice Husk Ash (RHA)	Calcined Clay (CC)	Portland Cement (PC)
SiO_2	83.34	59.22	20.25
Al_2O_3	1.46	15.57	4.88
Fe_2O_3	1.37	9.86	3.38
CaO	1.34	1.54	62.86
MgO	1.88	0.85	2.54
SO_3	0.20	0.03	2.75
K_2O	2.49	4.73	0.28
Na_2O	0.17	3.21	0.36
LOI	2.87	2.89	1.38
Specific gravity	2.13	2.59	2.95
Sum (SiO_2 , Al_2O_3 , Fe_2O_3)	86.17	84.65	

The details of the mix design for different concrete mixes are given in Table 2. The design was chosen to achieve a minimum compressive strength class of C20/25. The starting materials were mixed at a water-to-binder (w/b) ratio of 0.5 and by replacing 50% wt. and 60% wt. of PC with different proportions of RHA and CC. Increasing the SCM proportion resulted in a slight reduction in workability; however, the slump measured for all series was in the range of 55–105 mm, indicating a medium degree of workability. The series were labelled to reflect their binder composition (%) by mass (PC:CC:RHA). A control series, referred to as 100:00:00, with no SCM replacement, was also produced for comparison. A visual representation of the PC replacement level as a ternary plot is reported in Figure 2.

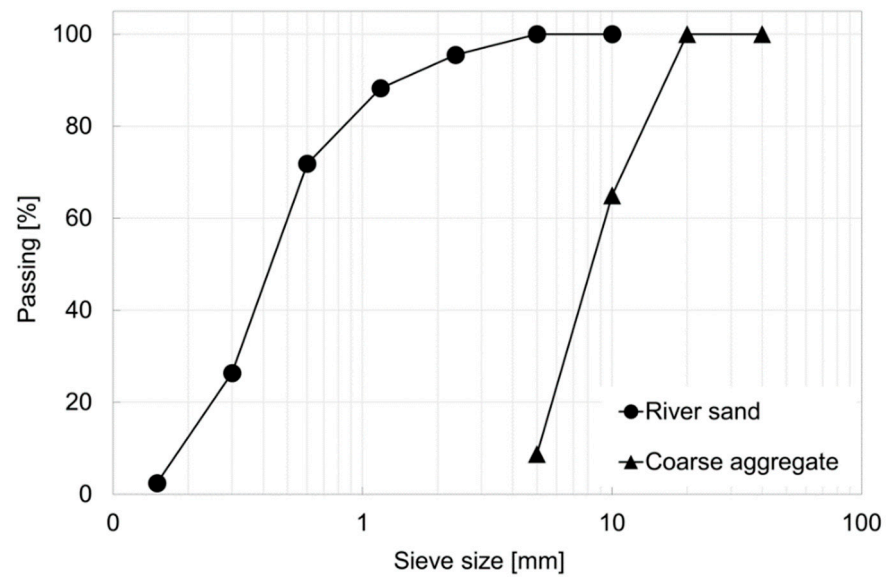


Figure 1. Particle size distribution of the fine (river sand) and coarse aggregates.

Table 2. Mix design of concrete mixes and ternary blend ratios by mass as PC:RHA:CC, where PC is Portland cement, RHA is rice husk ash, and CC is calcined clay.

Series	Blend	PC	RHA	CC	Aggregate	Sand	Water
ID	PC:RHA:CC	kg/m ³	kg/m ³	kg/m ³	kg/m ³	kg/m ³	kg/m ³
S1	100:00:00	342.9	0.0	0.0	1131.4	754.3	171.4
S2	50:50:00	171.4	171.4	0.0	1131.4	754.3	171.4
S3	50:40:10	171.4	137.2	34.3	1131.4	754.3	171.4
S4	50:25:25	171.4	85.7	85.7	1131.4	754.3	171.4
S5	50:10:40	171.4	34.3	137.2	1131.4	754.3	171.4
S6	50:00:50	171.4	0.0	171.4	1131.4	754.3	171.4
S7	40:50:10	137.2	171.4	34.3	1131.4	754.3	171.4
S8	40:35:25	137.2	120.0	85.7	1131.4	754.3	171.4
S9	40:10:50	137.2	34.3	171.4	1131.4	754.3	171.4

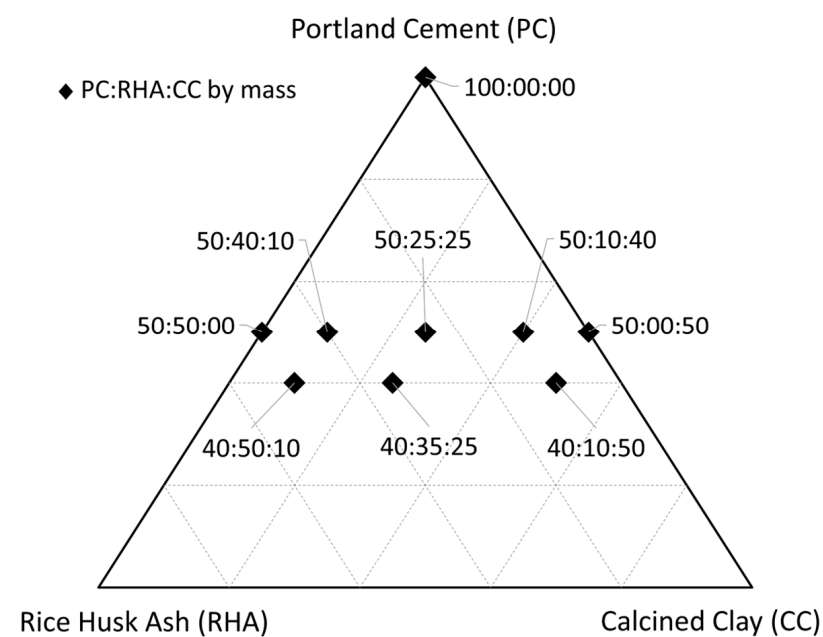


Figure 2. Ternary plot of blended cement replacements.

2.2. Methods

The concrete was cast according to the procedure described in ISO 1920-3:2019 [23]. Cube moulds of 150 mm in size were cast and kept for 24 h under a temperature of 20 ± 5 °C and relative humidity > 50%. After demoulding, the concrete cubes were cured under water and maintained at a temperature of 20 ± 2 °C, until an age of 28 days. Samples were tested for compressive strength, water absorption, open porosity, density, and pore size distribution to understand the influence of RHA and CC on concrete. To assess the impact of wet/dry cycles on aged concrete, specimens were placed in 3.5% NaCl solution for 12 h and then dried at 60 °C for 12 h. Immersion for 12 h and drying for 12 h is considered as one cycle of wetting and drying, adapted from similar studies [24,25]. Concrete samples were subjected to a total of 20 cycles and tested before and after wet/dry cycles as follows: The compressive strength and capillary water absorption of concrete were measured following ISO 1920-4:2019 standard [26] and ASTM C1585-2020, respectively [27]. Open porosity, bulk, and matrix density were measured following the methodology reported in BS EN 12390-7:2019 [28]. Thermogravimetric curves were collected using a Mettler Toledo (Leicester, UK) TGA/DSC3+, from ambient temperature to 1000 °C, at a heating rate of 10 °C/min under constant inert gas flow. A 20 mg powder sample, preconditioned in an oven for 3 days at 60 °C, was used. The pore size distribution of the samples was measured by mercury intrusion porosimetry using a Micromeritics (Norcross, GA, USA) AutoPore V (9620). Intrusion data were collected in the approximate applied pressure range of 0.3–60,000 psia with equilibration by time (10 s). Maximum mercury intrusion limits were set to 0.05 mL/g or lower to ensure the collection of a reasonable number of data points in regions of mercury intrusion. Low-pressure analysis was conducted to 45 psia and high-pressure analysis in the range of 45–60,000 psia. The surface tension of mercury was 480 dynes/cm, with a contact angle of 140 degrees. Scanning electron microscopy imaging and chemical analysis were carried out using a Zeiss Sigma (Moringen, Germany) HD FEG-SEM. Fragments of selected samples were mounted on carbon adhesive tabs on aluminium pin stubs before being carbon coated with 15 nm carbon using an Agar Turbo Carbon Coater (Agar Scientific, Essex, UK). Secondary electron (SE) imaging and energy dispersive spectroscopy (EDS) X-ray analysis were performed under high-vacuum conditions with a beam energy of 20 kV and a 60 µm diameter final aperture, with a resulting beam current of 1.5 nA. A dwell time of 20 µs per pixel was used for imaging with an Everhart–Thornley SE detector, and an acquisition time of 10 s was used for chemical analysis with a processing time of 3 µs. Thermal conductivity and electrical resistivity measurements were conducted to complement information on the microstructure of the sample and for a better understanding of the effect of wet/dry cycles on the specimens' durability. Thermal conductivity was measured using the TLS 50 mm probe (Thermtest MP2, Veddige, Sweden) in accordance with ASTM D5334-22 [29] at room temperature, on preconditioned samples. Bulk electrical resistivity was measured using the RCON apparatus (GIATEC, Ottawa, ON, Canada) at room temperature on samples subjected to saturation before testing [30].

3. Results

3.1. Compressive Strength

Figure 3 shows the compressive strength of the mixes before and after wet/dry cycles. It can be observed that replacing PC with 50% RHA resulted in approximately 60% loss in compressive strength, which is expected due to the dilution effect caused by the decreased amount of clinker in the mix. Previous studies have shown that 10% to 15% of RHA is optimal to achieve maximum long-term strength (90 days). Beyond the 20% replacement level, usually a significant decrease in the strength is reported, especially at early ages [31]. Delayed pozzolanic activity of RHA is generally considered responsible for this early-age compressive strength reduction [32]. Therefore, the strength of the RHA mix may improve when tested at later ages such as 90 days and beyond [33]. The addition of CC to the

mix moderately improved the compressive strength. This behaviour was prevalent with both 50% and 60% replacement ratios. The pozzolanic activity of CC is higher than that of RHA; therefore, an improvement in strength at early ages is visible. It has been reported that the kaolinite content of clays is majorly responsible for microstructure and strength development [34]. Despite the lower kaolinite and higher amount of quartz in the clay used, the addition of CC improved the strength. The strength of all the mixes moderately increased after wet/dry cycles. This is due to further hydration taking place during the wet/dry cycles and subsequent increased temperature during the drying period [24,25]. Furthermore, the presence of salts has been reported to activate the hydration of residual cement phases and pozzolanic reactions, resulting in increased strengths [35,36].

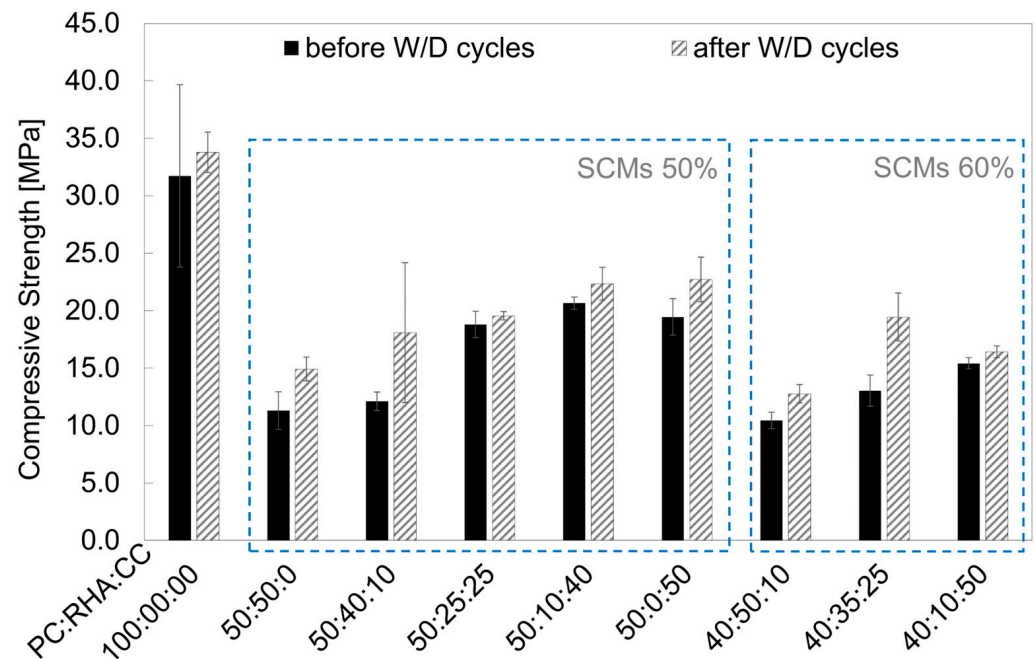


Figure 3. Comparison of compressive strength values of binary and ternary concrete mixtures with the control sample, before and after wet/dry (W/D) cycles.

At early ages, the nucleation effect of RHA accelerates hydration, giving a positive effect to early-age strength with a low dosage of RHA; however, limited participation of RHA in the hydration process gives a subsequent decrease in strength in the later stages because of the dilution effect. Besides the physical filling effect of CC, the participation of CC in the hydration process through pozzolanic effects resulted in an enhancement in strength. The silicon/aluminium compounds present in CC react with portlandite and contribute to the formation of C-S-H/C-(A)-S-H phases, thus making the matrix denser. Generally, SCMs with higher concentrations of active constituents and finer particle sizes exhibit a more robust pozzolanic effect. Here, CC outperforms and counter-balances RHA in terms of strength development. The concrete mix was designed for a minimum compressive strength class of C20/25, satisfied only by the samples in the control series. However, specimens with RHA and CC showed strength values > 10 MPa. This suggests that such concrete can be used for non-structural applications, such as slabs, pavements, filling, and insulation panels.

3.2. Sorptivity

The water absorption findings presented in Figure 4 highlight a significant impact of RHA and CC on the overall sorptivity. Specifically, concrete with 50% RHA exhibited water absorption rates five times higher than those of the control PC concrete. Mixes characterised by higher replacement levels and low PC content (SCMs 60%) showed increased sorption compared to counterparts with lower replacement levels (SCMs 50%). The introduction

of CC resulted in a noticeable decrease in water absorption. At both substitution levels (SCMs 50% and 60%), sorptivity is directly proportional to the CC content while inversely proportional to the RHA content. This may be attributed to the pozzolanic reactions of CC, which contributed to decreasing capillary connectivity and refining the pore structure within the binders. The sorptivity of concrete incorporating only CC (series PC:RHA:CC 50:00:50) was 50% higher than that of 100% PC only after chloride attacks under wet/dry cycles. However, concrete incorporating RHA showed a relative increase in sorptivity compared to both control concrete and CC concrete. The synergistic effect of RHA and CC contributed to an overall reduction in sorptivity.

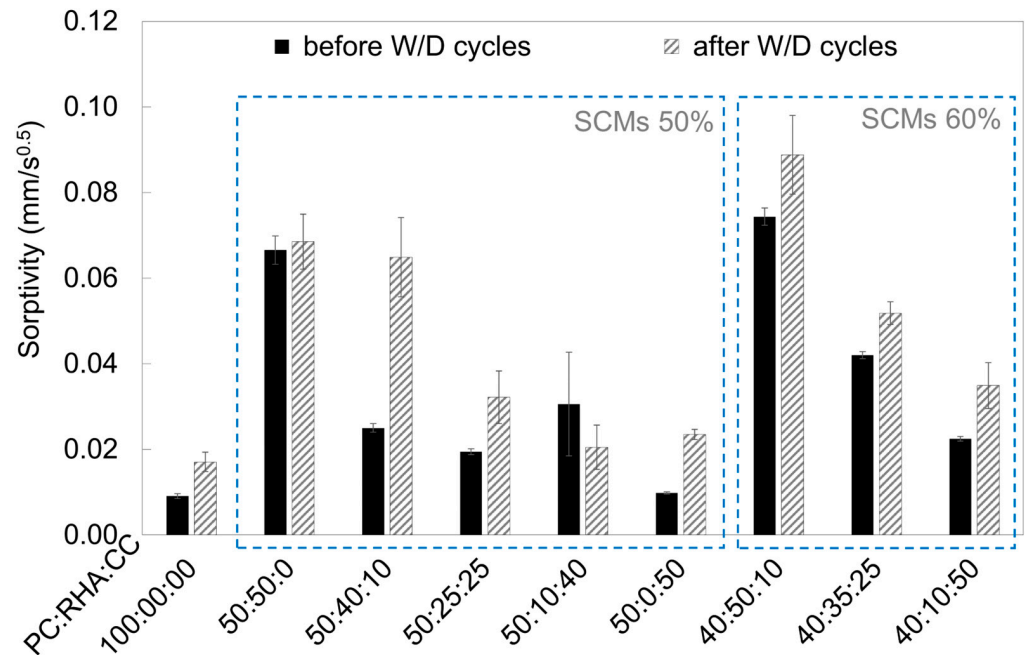


Figure 4. Comparison of sorptivity values of binary and ternary concrete mixtures compared to the control sample, before and after wet/dry (W/D) cycles.

CC has been reported to yield dense microstructures, resulting in a finer pore structure and lower sorption through concrete [37]. Further analysis revealed that increasing the amount of CC further reduced sorption, leading to the least absorption at 50% CC. Figure 4 illustrates the sorptivity values of all the samples before and after exposure to NaCl solution during wet and dry cycles. It can be observed that subjecting the samples to wet/dry cycles increased sorption through mixes, except for 40% CC. The results show a significant rise in levels of sorptivity for the samples undergoing cyclic wetting and drying. One reason for this subsequent increase could be the dissolution of hydrates and carbonates in concrete [38]. Another reason for this behaviour could be the probability of crack formation due to drying at higher temperatures. Microcracks are known to have a greater influence on transport through concrete [36].

3.3. Open Porosity and Density

Figure 5 demonstrates that the addition of RHA to concrete significantly increases open porosity, which can be attributed to the lower amount of hydration products expected in these mixes due to the reduced amount of clinker. Lower substitution levels (<20%) have been reported to decrease porosity, whereas high substitution with RHA is observed to increase porosity due to the low pozzolanic activity of RHA. The addition of CC to RHA mixes was shown to lower the values of open porosity, demonstrating the contribution of CC to microstructure development. Similar results have been reported using silica fume and nano CaO for combined substitution with RHA [33,39]. Wet/dry cycles have a negligible influence on open porosity, whereas sorptivity increases after being subjected to

wet/dry cycles. This indicates that the open porosity measurement under vacuum might not detect changes at the micropore level caused by the penetration of saline water and subsequent crystallization and/or formation of hydration products in existing pores [40,41]. Therefore, the pore structure was also evaluated using a mercury intrusion porosimeter.

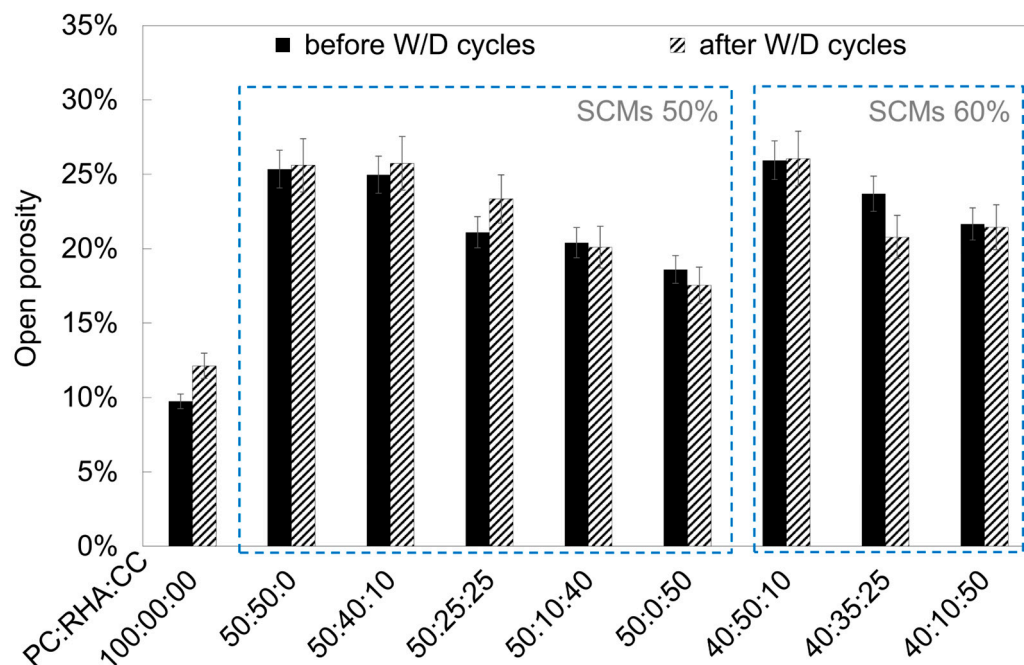


Figure 5. Comparison of open porosity values of binary and ternary concrete mixtures with control sample, before and after wet/dry (W/D) cycles.

The reason behind the high porosity can be related to the abundance of gel pores developed in the microstructure, whereas low-porosity concrete has additional C-S-H phases that inhibit porosity. Furthermore, the available pores play an important role in shaping clinker reactions as well as the chemical composition of the C-S-H [42]. These microstructure modifications are suggested by Haha et al. [43] to also show high-porosity behaviour that can lower the Ca/Si ratio. In the present study, RHA and CC react slower than the cement clinker and may contribute to the refinement of microstructure at later ages.

3.4. Thermal Conductivity and Bulk Electrical Resistivity

Figure 6 shows the thermal conductivity of mixes before and after wet/dry cycles. Control cement specimens showed the highest thermal conductivity before wet/dry cycles, whereas the addition of 50% RHA significantly reduced the conductivity. SCMs are known to increase the air content and decrease the density, which decreases the heat transfer rate of concrete. Thus, a decrease in the thermal conductivity of the 50% RHA mix is expected, owing to its higher porosity and lower density. All the mixes containing CC showed similar thermal conductivity values which are slightly higher than the thermal conductivity of the 50% RHA mix. The lower porosity and slightly higher density of the mixes containing CC compared to the RHA mix might have contributed to the increased thermal conductivity of these mixes.

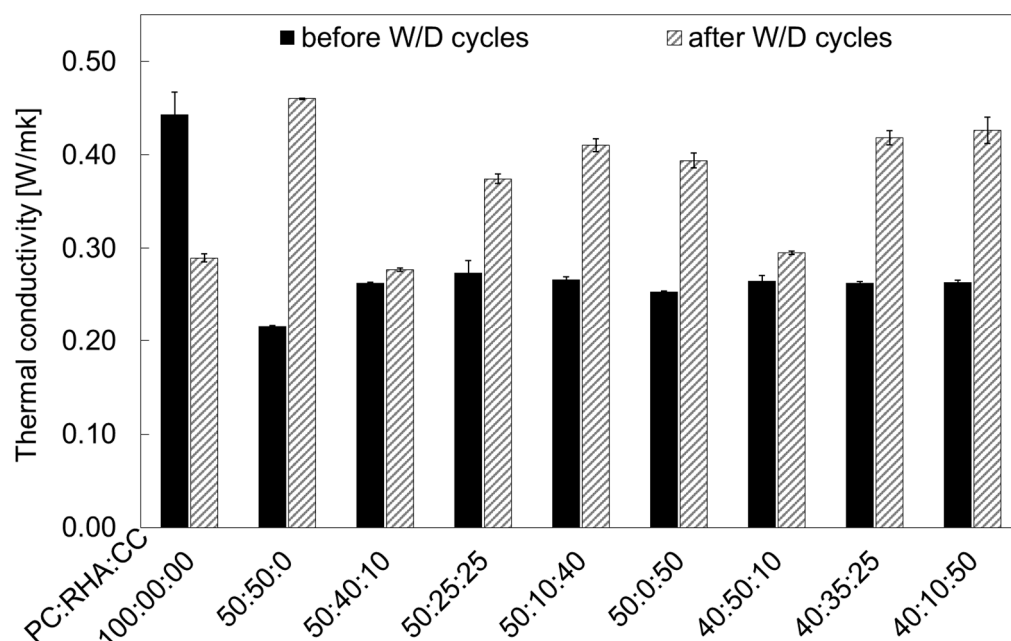


Figure 6. Comparison of thermal conductivity of binary and ternary concrete mixtures with the control sample, before and after wet/dry (W/D) cycles.

Relative to cement, RHA and CC have a high silica content and lower specific gravity, thus contributing to a reduction in thermal conductivity, as evidenced by Raheem et al. [44] and Khushefati et al. [45]. The findings from the present study affirm that the incorporation of RHA and CC contributes to enhancing the thermal insulation properties of concrete, having a noteworthy impact on the energy consumed in a building. The indoor temperature of a building can be reduced with the application of RHA and CC, owing to low heat conduction from outside in hot weather conditions. Curing and time are also important factors that may affect the thermal conductivity of RHA and CC blended concrete, according to Raheem et al. [44]. With the increase in curing ages, thermal conductivity may increase due to additional hydration products formed by the filling of voids between concrete particles, thus enhancing concrete density. This dynamic interaction over time underscores the importance of considering curing effects in optimising the thermal performance of RHA and CC blended concrete.

After wet/dry cycles, an increase in thermal conductivity is recorded for all SCM series. This is due to the higher porosity induced by the accelerated aging and subsequent crystallisation of NaCl phases into the available pores.

The results of the bulk electrical resistivity measurements are summarised in Figure 7. Values of electrical resistivity higher than 8–16 kΩ cm are comparable to low chloride penetration measured with the standard rapid chloride permeability (RCP) test [33]. Twenty-eight-day aged samples show a relatively high degree of electrical resistivity (>16 kΩ cm), suggesting that the chloride penetration can be considered very low or negligible [30]. However, after wet/dry cycles, all samples showed a significant drop in electrical resistivity due to the internal damage caused by salt crystallisation, subsequent microcracking, and salt precipitation. For series with 40% PC, the electrical resistivity is proportional to the CC content and inversely proportional to the RHA one, as shown in Figure 8. This can be attributed to the denser microstructure produced by the addition of CC.

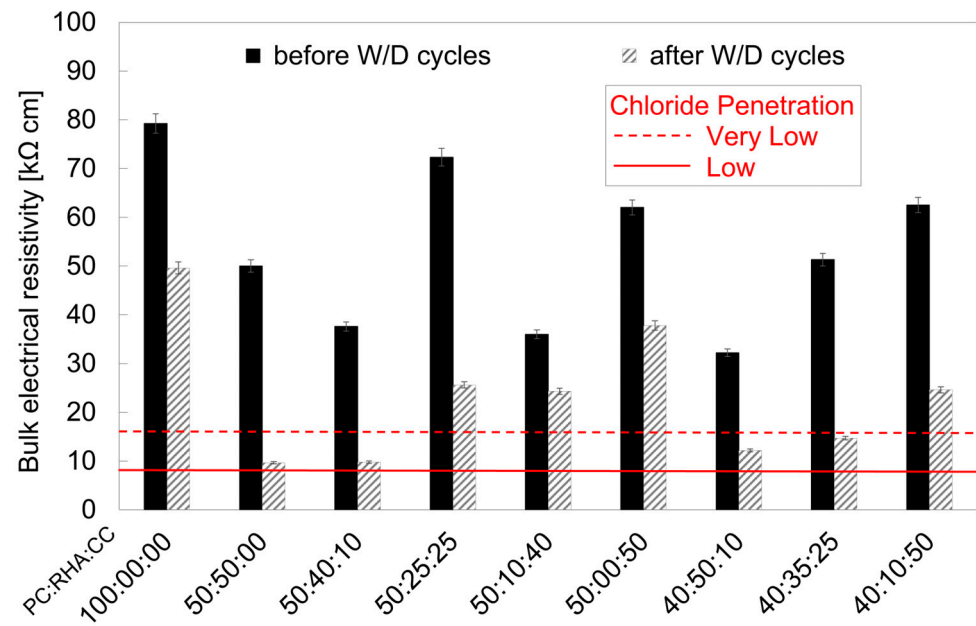


Figure 7. Bulk electrical resistivity of samples before and after exposure to wet/dry (W/D) cycles.

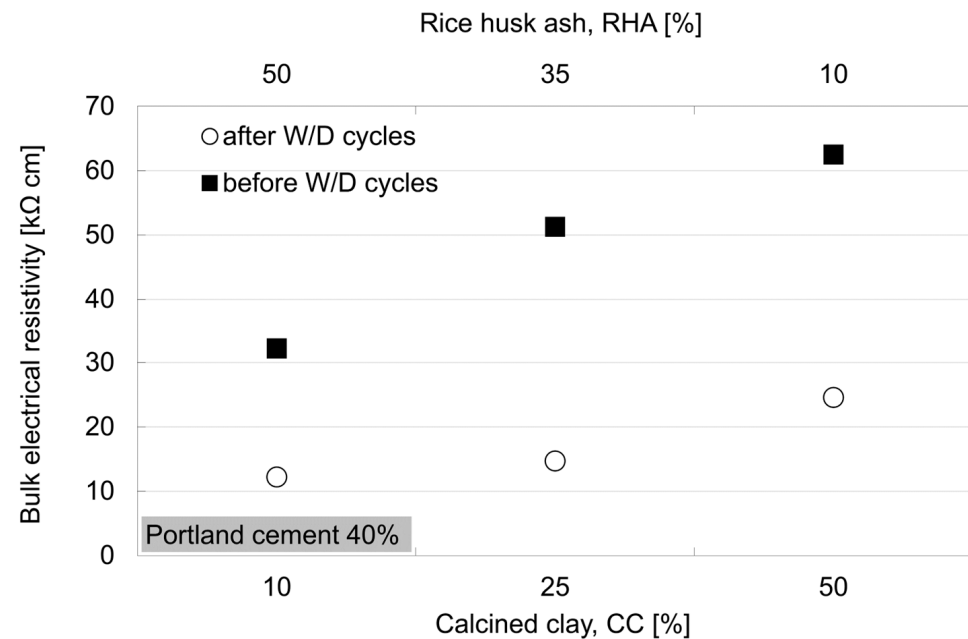


Figure 8. Bulk electrical resistivity of samples before and after exposure to wet/dry (W/D) cycles as a function of the calcined clay (CC) content and rice husk ash (RHA) content.

The electrical resistivity of concrete directly depends on the permeability property of the concrete, pore interconnectivity in concrete microstructure, and the ionic composition of the pore solution [46]. The higher the ionic transport in the concrete, the lower the electric resistivity. However, this gives rise to the penetration of destructive ions, likely Cl^- , responsible for the initiation of corrosion in steel reinforcement bars. In the present study, CC mixes attained higher resistivity relative to RHA mixes. When comparing PC mixtures with CC and RHA mixtures, the two key insights are that the formation of hydration products not only has a significant impact on compressive strength but also has a notable influence on pore connectivity and pore size distribution. Secondly, the addition of SCMs may impact the concentration of ions in pore solution, thus reducing the electrical conductivity of concrete. This reduction could potentially introduce a source of error in assessing concrete permeability through electrical-based methods [46,47]. These

phenomena jointly resulted in a relative decrease in electrical resistivity in blended mixtures, however yet in the range of very low chloride penetration [48].

3.5. Microstructure Characterisation

The distribution of pore volume was investigated using MIP measurements in PC mixtures, as well as mixtures containing RHA and CC after a 28-day curing period, as illustrated in Figure 9. Three distinct types of pores, categorised by pore diameters, were identified based on the existing literature [49,50]: air pores ranging from 10 to 100 μm , mesopores spanning 0.1–10 μm , and micropores within the 0.005–0.1 μm range (encompassing gel pores smaller than 0.01 μm). Differential intrusion profiles define critical pore entry size as the diameter of the peak [51]. Overall, the hydration process led to a reduction in the total pore volume across all mixtures, attributed to an increased production of hydration products.

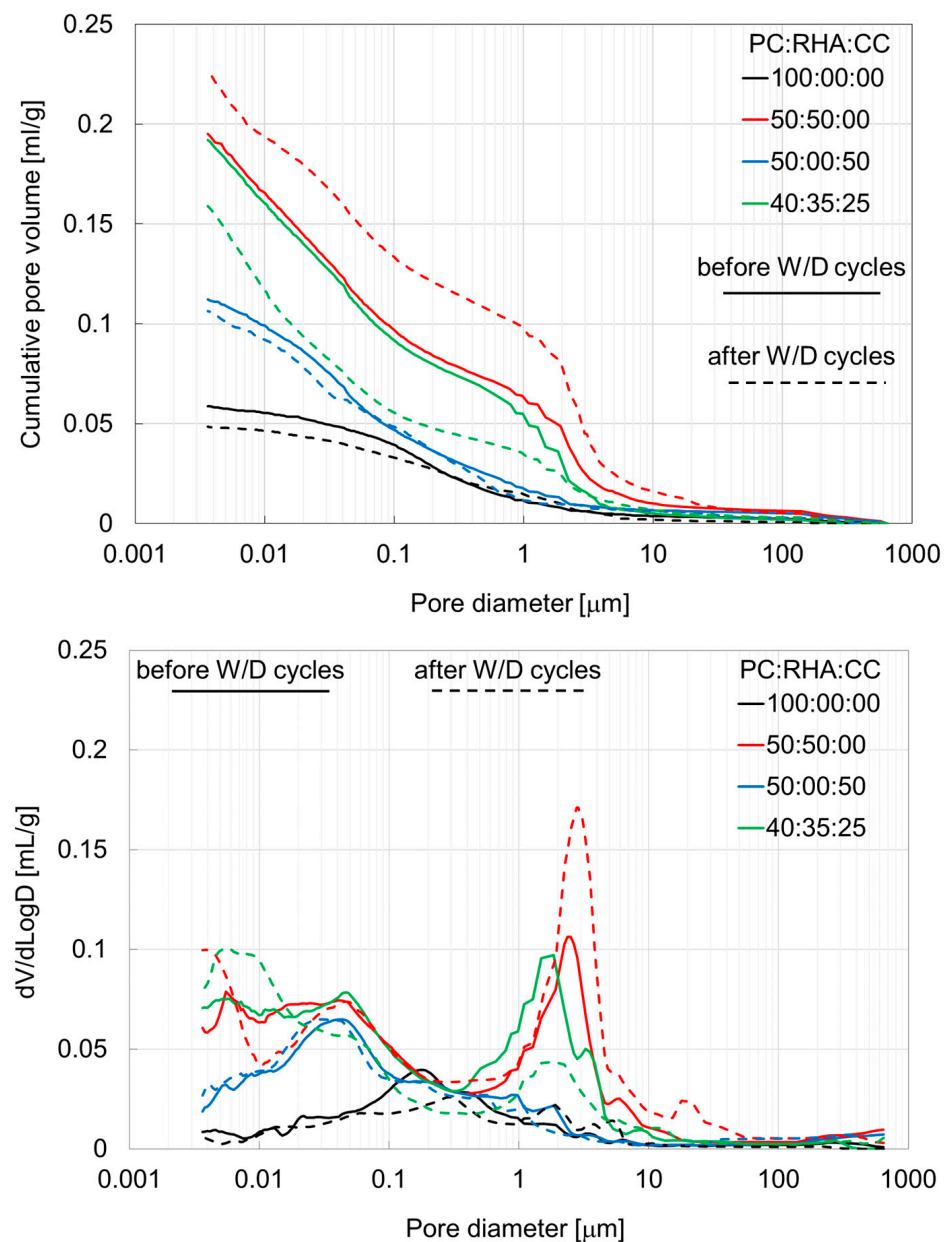


Figure 9. Influence of RHA and CC substitution on the pore size distribution as a function of the pore volume (**top**) and as a function of the $dV/d\text{Log}D$ (**bottom**), before and after wet/dry (W/D) cycles.

Figure 9 shows the pore size distribution and differential intrusion volume for the selected mixes. The total intruded volume significantly increased with the use of RHA. Mixes with CC also showed a higher total intruded volume compared to the mixes with only PC. However, the critical pore size is significantly lower in the CC mix compared to the plain PC mix. Mixes with RHA showed two peaks, one between 1 and 10 μm and the other within pore size less than 0.1 μm . The first peak generally corresponds to the capillary pores, whereas the second peak corresponds to the gel pores. The comparison of differential intrusion volumes of different mixes suggests that the mixes with RHA have a higher volume of capillary pores compared to PC and CC mixes.

The use of supplementary cementitious materials is known to influence the microstructure. Figure 10 shows the distribution of the volume of pores of different size in the selected mixes. It is clearly visible that RHA increases the volume of pores ranging between 1 and 10 μm and less than 0.1 μm in size. Mixes with CC 50% showed a higher number of pores below 0.1 μm in size. The higher total intruded volume and higher number of capillary-sized pores in RHA mixes justify the higher sorptivity in these mixes (as shown in Figure 4). The total intruded volume increased for the mix containing 50% RHA after wet/dry cycles and decreased for the series at a 60% SCM replacement level (PC:RHA:CC 40:35:25), in line with open porosity data, whereas for the other two series, the influence of wet/dry cycles on the pore structure seemed to be negligible.

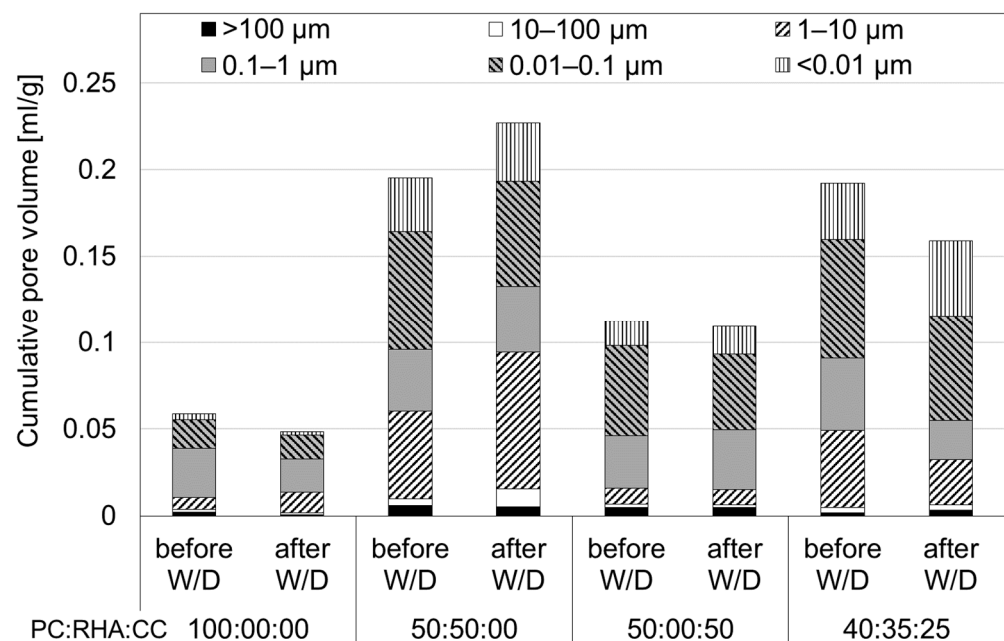


Figure 10. Change in the pore sizes due to substitution and wet/dry cycles (W/D).

As illustrated in Figure 10, a notable reduction in the volume of mesopores after wet/dry cycles can be observed for samples containing RHA and CC. This reduction might be attributed to the continued hydration of RHA and CC during the wetting stage. The volume of micropores and gel pores showed a significant improvement. This might be due to the presence of interlayer pores in C-A-S-H phases as well as the formation of ettringite.

Figure 11 illustrates selected thermogravimetric curves for the control series and for the 50% RHA, 50% CC, and PC-RHA-CC blended specimens. Three distinct thermal steps can be identified: The initial section spans from a range of 50–250 $^{\circ}\text{C}$ approximately, corresponding to the relative mass change associated with the dehydration of pore water and C-S-H. The thermal range 400–500 $^{\circ}\text{C}$ is primarily associated with the dehydroxylation of portlandite. The final section, 680–800 $^{\circ}\text{C}$, represents the mass change due to the decomposition of carbonates. A significant increase in mass loss after wet/dry cycles in the first thermal step (C-S-H/C-A-S-H) is recorded for series with RHA and CC, suggesting

the additional formation of hydrated products. This confirms that water available during the wetting stage contributed to continued hydration and pozzolanic reactions. Similarly, the thermal step associated with portlandite is negligible when CC and RHA are used, suggesting that the available calcium hydroxide has been consumed to form additional C-S-H/C-A-S-H phases [52].

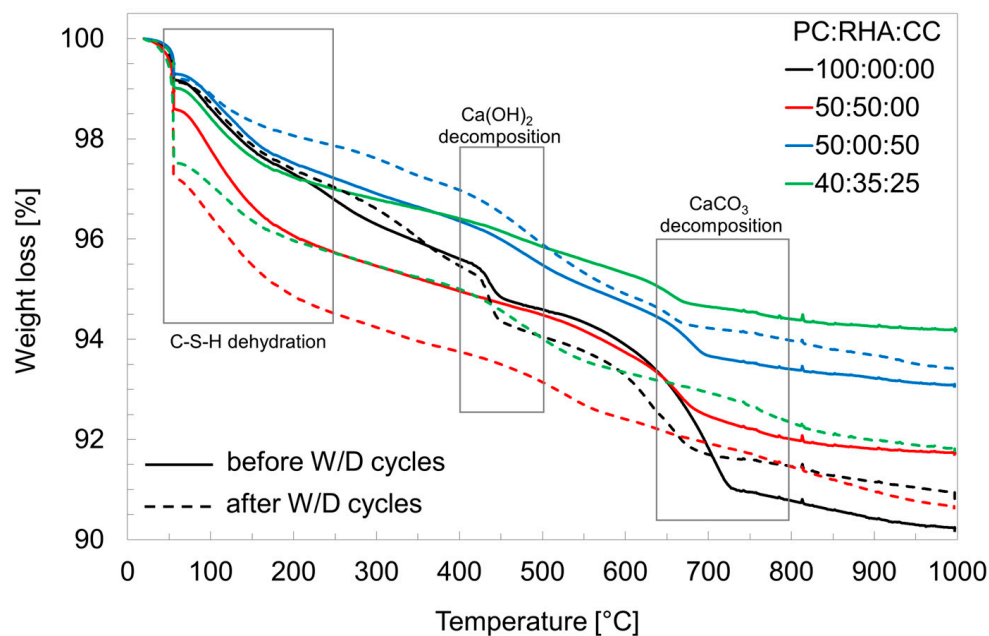


Figure 11. Thermogravimetric response of selected samples before and after exposure to wet/dry (W/D) cycles.

Figure 12 shows the XRD patterns of selected series (control, 50% RHA, 50% CC, and PC-RHA-CC blended specimens) before and after wet/dry cycles. Hydration products (C-S-H), portlandite, and calcite were observed as a result of the hydration process and ageing. The typical chloride ion attack product, Friedel's salt, $C_3A \cdot CaCl_2 \cdot 10H_2O$, also appeared in the hydration products. The Friedel's salt main diffraction peaks were absorbed at 11.16° , 39.58° , and 41.3° 2θ . This salt was prevalent within the series with the higher CC content. Previous studies have shown that high-alumina-containing materials such as FA and GGBFS show a higher binding affinity for the Friedel's salt. The alumina in the SCMs reacts with the chloride ions to form Friedel's salt, which indicates the main mechanism of improving the chloride binding capacity for mixes with CC and RHA. The amount of Friedel's salt observed increased with an increase in the amount of CC added to the concrete. In the control series, the Friedel's salt peaks were not as defined as the ones found in specimens containing RHA and CC. Previous studies have shown that Friedel's salt could further result from the physical adsorption of the chloride ion by the C-S-H phase in the cement hydration product. This would explain the relatively small peaks observed in the control series.

The XRD pattern showed well-defined peaks corresponding to various compounds, including C-A-S-H, quartz, alite, belite, portlandite, calcite, C-S-H, and Friedel's salt. Incomplete hydration can be observed in the binder paste due to the presence of peaks associated with alite, belite, and quartz. Ternary mixes PC:RHA:CC 50:25:25 and 40:35:25 exhibited less intense peaks of alite, belite, and quartz relative to the binary mix PC:RHA:CC 50:00:50. However, after wet/dry cycles, mixes showed a reduced intensity of such peaks, suggesting that a higher degree of hydration was achieved.

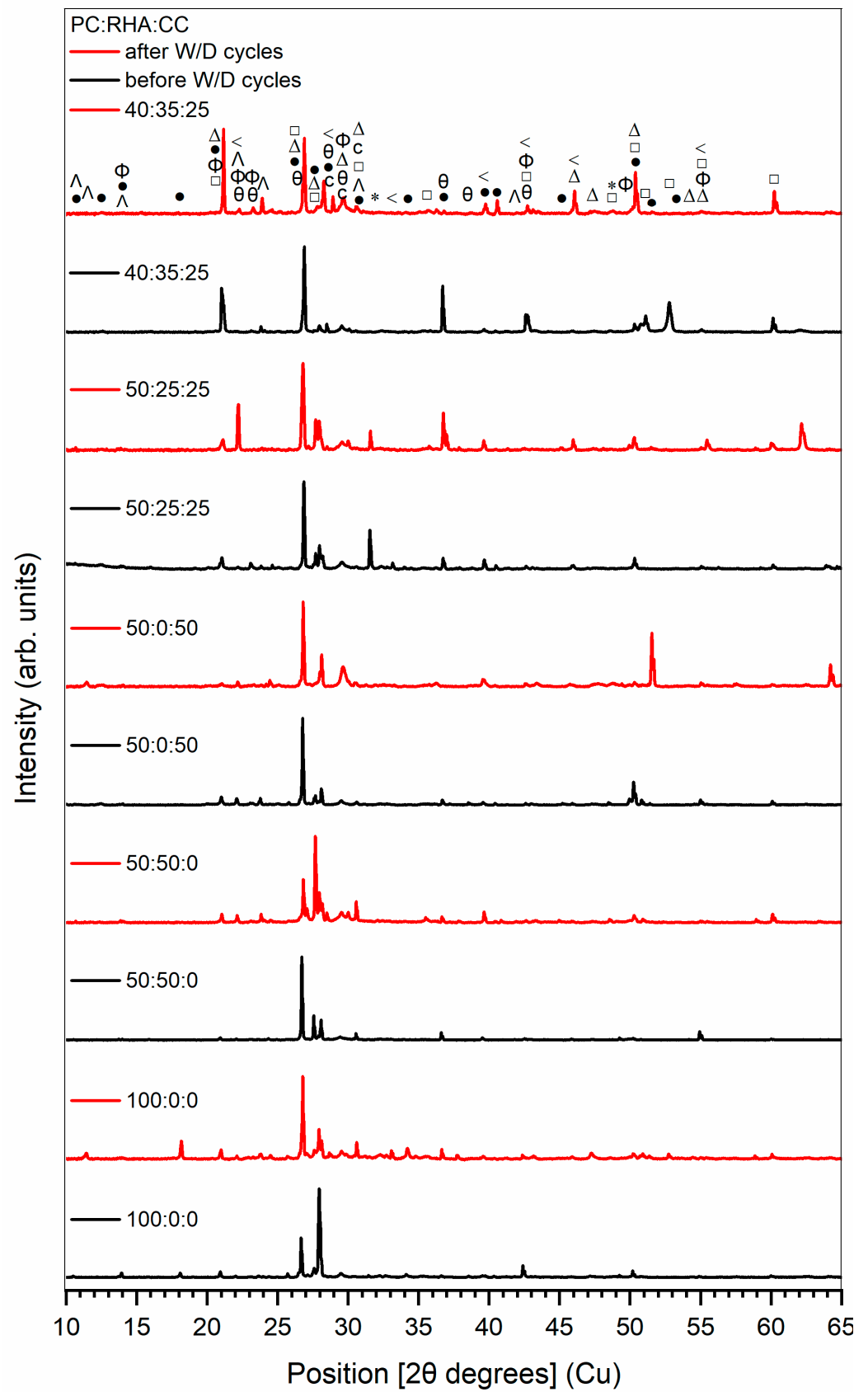


Figure 12. XRD analysis of samples after wet/dry (W/D) cycles (Δ : calcium aluminium silicate hydrate; $<$: CAH; \square : quartz; Φ : alite; $*$: belite; \bullet : portlandite; θ : calcite; c: CSH; Λ : Friedel's salt).

Conversely, qualitative comparison of XRD patterns showed a higher intensity of peaks associated with C-S-H and C-A-S-H in ternary blends. The silica and aluminium available in RHA and CC, respectively, react with the calcium hydroxide formed during the hydration of PC, leading to the development of additional C-S-H (or C-A-S-H) phases.

Figure 13 presents SEM images of selected series before and after wet/dry cycles, the control series and a ternary blend series (PC:RHA:CC 100:00:00 and 50:40:10). The images of the control series before wet/dry cycles depict a relatively compact surface with only a few pores and microcracks in the concrete matrix. However, after wet/dry cycles, the matrix exhibits irregular microcracks and micropores due to drying shrinkage and salt crystallisation which occurred during the wetting and drying stages. This sheds light on the potential reasons behind the reduced strength of concrete under such environmental conditions. The presence of hydration products is confirmed by EDX analysis (detection of Ca, Si, and O), supporting the findings from the XRD analysis. The hydration process appears to be amplified by the addition of RHA and CC, leading to an improvement in the microstructure of the specimens. As observed in the SEM micrographs, a compact and uniform composition is evident for specimens in series 50:40:10 compared to the control. This can be attributed to the development of C-S-H phases and RHA's filler effect. In contrast, the control specimen displays the presence of C-S-H phases alongside voids. These observations underscore the positive impact of incorporating CC and RHA on the microstructural properties of concrete, emphasising the role of these SCMs in enhancing the overall matrix refinement.

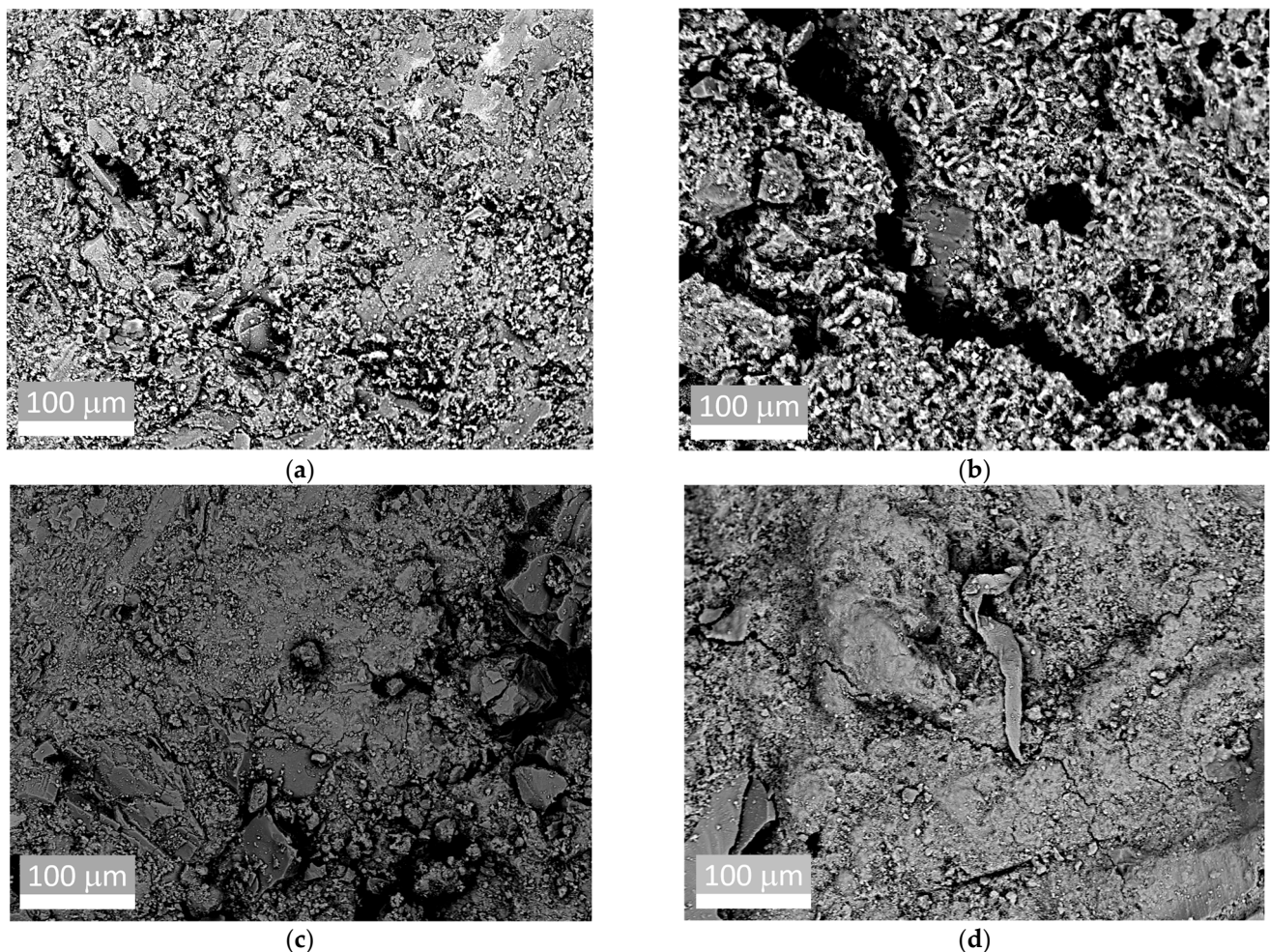


Figure 13. Scanning electron microscopy (SEM) images of control specimen PC:RHA:CC 100:00:00 (a) before and (b) after wet/dry cycles and specimen PC:RHA:CC 50:40:10 (c) before and (d) after wet/dry cycles.

4. Conclusions

While the durability of concrete incorporating conventional supplementary cementitious materials (SCMs) such as silica fume, fly ash, and GGBS has been extensively studied, the long-term properties of innovative ternary blends involving Portland cement, rice husk ash (RHA), and calcined clay (CC) have not been fully explored. This work aims to provide valuable insights into the durability performance of ternary blended concretes using locally available resources in Kenya.

This study investigates the strength and durability of concrete mixes incorporating Portland cement (PC) and varying contents (up to 50% by weight) of RHA and CC in ternary blends. The impact of accelerated durability testing under wet/dry cycles in saline water, as a function of RHA and CC content, is also assessed. While a 50% RHA replacement resulted in a notable decrease in compressive strength, the combined use of CC mitigated this loss. The strength of all mixes remained largely unaffected after wet/dry cycles. The higher pozzolanic reactions of CC contributed to a decrease in water absorption, albeit slightly higher than the control concrete. However, the introduction of RHA led to a subsequent increase in sorptivity relative to both the control and CC series. The synergistic effect of RHA and CC yielded satisfactory results. The relatively higher permeability of CC compared to RHA mixtures is primarily due to the pozzolanic effect of calcined clay, leading to the formation of pozzolanic hydrates.

A notable reduction in the volume of mesopores after wet/dry cycles was observed for samples containing RHA and CC, attributed to the continuous reactions of RHA and CC. Interestingly, the volume of micropores and gel pores showed significant improvement, likely due to the presence of interlayer pores in C-A-S-H phases and the abundant formation of ettringite. Comparative analysis of ternary mixes highlighted that RHA-CC blended concrete exhibited lower amounts of unhydrated phases and higher amounts of C-S-H and C-A-S-H phases. Silica available in CC and calcium hydroxide produced from the hydration of PC led to heightened development of the C-S-H phase. This reaction enhanced compressive strength through the formation of C-A-S-H phases.

In conclusion, the introduction of RHA into the concrete mix resulted in a notable decrease in the overall properties of concrete; however, the synergistic effect of RHA and CC showed satisfactory results, prompting further investigation with replacement levels below 50% of OPC. Due to the delayed pozzolanic reactivity of SCMs, further investigations are needed to evaluate strength and durability properties at later ages, such as 56 and 90 days, when the full reaction of CC and RHA is achieved. Further studies are also required to investigate ternary blends with high-kaolinite clays to optimise the RHA mixes and maximise the Ca/Si ratio.

Author Contributions: Conceptualisation, J.M.M. and R.M.; methodology, J.M.M. and R.M.; validation, M.S., L.S., V.I.N. and V.K.M.; formal analysis, I.K., E.L. and D.K.A.; investigation, J.M.M., R.M., M.S. and V.K.M.; resources, J.M.M., M.S. and R.M.; data curation, R.M., J.M.M., M.S., L.S. and V.K.M.; writing—original draft preparation, J.M.M., V.K.M., M.S. and R.M.; writing—review and editing, M.S., L.S., V.K.M., D.K.A., E.L., I.K., V.I.N., J.M.M. and R.M.; visualisation, R.M. and D.K.A.; supervision, R.M., E.L. and V.I.N.; project administration, R.M. and J.M.M.; funding acquisition, R.M., J.M.M. and E.L. All authors have read and agreed to the published version of this manuscript.

Funding: This research was funded by the HEFCW GCRF funded fellowship through Cardiff University: “Circular Cement: local resources for affordable and sustainable infrastructures in Kenya”, and the APC was funded by Cardiff University. The Czech Science Foundation, under project No 22-04726S, is also acknowledged.

Data Availability Statement: The datasets generated and analysed for this study can be found in the Cardiff University repository at <http://doi.org/10.17035/d.2022.0161507818>.

Acknowledgments: The Cardiff University Engin Research Boost Grant 2022 allowed for electrical resistivity measurements.

Conflicts of Interest: The authors declare no conflicts of interest. The funders had no role in the design of this study; in the collection, analyses, or interpretation of data; in the writing of this manuscript; or in the decision to publish the results.

References

1. Lin, X.; Li, W.; Guo, Y.; Dong, W.; Castel, A.; Wang, K. Biochar-Cement Concrete toward Decarbonisation and Sustainability for Construction: Characteristic, Performance and Perspective. *J. Clean. Prod.* **2023**, *419*, 138219. [[CrossRef](#)]
2. Danish, A.; Ozbakkaloglu, T. Greener Cementitious Composites Incorporating Sewage Sludge Ash as Cement Replacement: A Review of Progress, Potentials, and Future Prospects. *J. Clean. Prod.* **2022**, *371*, 133364. [[CrossRef](#)]
3. Monteiro, P.J.M.; Miller, S.A.; Horvath, A. Towards Sustainable Concrete. *Nat. Mater.* **2017**, *16*, 698. [[CrossRef](#)]
4. Arbelaez Perez, O.F.; Florez, D.R.; Zapata Vergara, L.M.; Hernández Benavides, K.V. Innovative Use of Agro-Waste Cane Bagasse Ash and Waste Glass as Cement Replacement for Green Concrete. Cost Analysis and Carbon Dioxide Emissions. *J. Clean. Prod.* **2022**, *379*, 134822. [[CrossRef](#)]
5. Aksoylu, C.; Özkılıç, Y.O.; Bahrami, A.; Yıldız, S.A.; Hakeem, I.Y.; Özdöner, N.; Başaran, B.; Karalar, M. Application of Waste Ceramic Powder as a Cement Replacement in Reinforced Concrete Beams toward Sustainable Usage in Construction. *Case Stud. Constr. Mater.* **2023**, *19*, e02444. [[CrossRef](#)]
6. Zhang, Y.; Zhang, L.; Wang, Q.; Han, D.; Li, Z. Iron Ore Tailings, Phosphate Slags, and Lithium Slags as Ternary Supplementary Cementitious Materials for Concrete: Study on Compression Strength and Microstructure. *Mater. Today Commun.* **2023**, *36*, 106644. [[CrossRef](#)]
7. Juenger, M.C.G.; Snellings, R.; Bernal, S.A. Supplementary Cementitious Materials: New Sources, Characterization, and Performance Insights. *Cem. Concr. Res.* **2019**, *122*, 257–273. [[CrossRef](#)]
8. Charitha, V.; Athira, V.S.; Jittin, V.; Bahurudeen, A.; Nanthagopalan, P. Use of Different Agro-Waste Ashes in Concrete for Effective Upcycling of Locally Available Resources. *Constr. Build. Mater.* **2021**, *285*, 122851. [[CrossRef](#)]
9. Chen, K.-T.; Wang, J.-X.; Dai, Y.-M.; Wang, P.-H.; Liou, C.-Y.; Nien, C.-W.; Wu, J.-S.; Chen, C.-C. Rice Husk Ash as a Catalyst Precursor for Biodiesel Production. *J. Taiwan Inst. Chem. Eng.* **2013**, *44*, 622–629. [[CrossRef](#)]
10. Noaman, M.A.; Karim, M.R.; Islam, M.N. Comparative Study of Pozzolanic and Filler Effect of Rice Husk Ash on the Mechanical Properties and Microstructure of Brick Aggregate Concrete. *Heliyon* **2019**, *5*, e01926. [[CrossRef](#)]
11. Van Tuan, N.; Ye, G.; Van Breugel, K.; Copuroglu, O. Hydration and Microstructure of Ultra High Performance Concrete Incorporating Rice Husk Ash. *Cem. Concr. Res.* **2011**, *41*, 1104–1111. [[CrossRef](#)]
12. Fapohunda, C.; Akinbile, B.; Shittu, A. Structure and Properties of Mortar and Concrete with Rice Husk Ash as Partial Replacement of Ordinary Portland Cement—A Review. *Int. J. Sustain. Built Environ.* **2017**, *6*, 675–692. [[CrossRef](#)]
13. Givi, A.; Abdul Rashid, S.; Nora, F.; Abdul aziz, F.; Amran, M.; Salleh, A. Contribution of Rice Husk Ash to the Properties of Mortar and Concrete: A Review. *J. Am. Sci.* **2010**, *6*, 157–165.
14. Rodríguez De Sensale, G. Effect of Rice-Husk Ash on Durability of Cementitious Materials. *Cem. Concr. Compos.* **2010**, *32*, 718–725. [[CrossRef](#)]
15. Scrivener, K.; Martirena, F.; Bishnoi, S.; Maity, S. Calcined Clay Limestone Cements (LC3). *Cem. Concr. Res.* **2018**, *114*, 49–56. [[CrossRef](#)]
16. Cancio Díaz, Y.; Sánchez Berriel, S.; Heierli, U.; Favier, A.R.; Sánchez Machado, I.R.; Scrivener, K.L.; Martirena Hernández, J.F.; Habert, G. Limestone Calcined Clay Cement as a Low-Carbon Solution to Meet Expanding Cement Demand in Emerging Economies. *Dev. Eng.* **2017**, *2*, 82–91. [[CrossRef](#)]
17. Alujas, A.; Fernández, R.; Quintana, R.; Scrivener, K.L.; Martirena, F. Pozzolanic Reactivity of Low Grade Kaolinitic Clays: Influence of Calcination Temperature and Impact of Calcination Products on OPC Hydration. *Appl. Clay Sci.* **2015**, *108*, 94–101. [[CrossRef](#)]
18. Obura, J.; Ombok, B.; Omugah, G. Analysis of Rice Supply Chain in Kenya. *Int. J. Manag. Stud. Res.* **2017**, *5*, 12–17. [[CrossRef](#)]
19. Schaefer, C.E.G.R.; Fabris, J.D.; Ker, J.C. Minerals in the Clay Fraction of Brazilian Latosols (Oxisols): A Review. *Clay Miner.* **2008**, *43*, 137–154. [[CrossRef](#)]
20. Oyebanjo, O.O.; Ekosse, G.E.; Odiyo, J.O. Mineralogy and Geochemistry of Clay Fractions in Soils Developed from Different Parent Rocks in Limpopo Province, South Africa. *Heliyon* **2021**, *7*, e07664. [[CrossRef](#)]
21. ASTM C150-07; Standard Specification for Portland Cement. Standards & Publications: West Conshohocken, PA, USA, 2012.
22. ASTM C618-19; Standard Specification for Coal Fly Ash and Raw or Calcined Natural Pozzolan for Use in Concrete. Standards & Publications: West Conshohocken, PA, USA, 2019.
23. ISO 1920-3:2019; Testing of Concrete, Part 3: Making and Curing Test Specimens. International Organization for Standards: Geneva, Switzerland, 2019.
24. Liu, F.; Zhang, T.; Luo, T.; Zhou, M.; Zhang, K.; Ma, W. Study on the Deterioration of Concrete under Dry-Wet Cycle and Sulfate Attack. *Materials* **2020**, *13*, 4095. [[CrossRef](#)] [[PubMed](#)]
25. Liu, X.; Ma, E.; Liu, J.; Zhang, B.; Niu, D.; Wang, Y. Deterioration of an Industrial Reinforced Concrete Structure Exposed to High Temperatures and Dry-Wet Cycles. *Eng. Fail. Anal.* **2022**, *135*, 106150. [[CrossRef](#)]
26. ISO 1920-4:2019; Testing of Concrete, Part 4: Strength of hardened concrete. International Organization for Standards: Geneva, Switzerland, 2019.

27. ASTM C1585-20; Standard Test Method for Measurement of Rate of Absorption of Water by Hydraulic-Cement Concretes. Standards & Publications: West Conshohocken, PA, USA, 2020.
28. BS EN 12390-7; Testing Hardened Concrete—Density of Hardened Concrete. British Standards Institution: London, UK, 2019.
29. ASTM D5334-22; Standard Test Method for Determination of Thermal Conductivity of Soil and Rock by Thermal Needle Probe Procedure. Standards & Publications: West Conshohocken, PA, USA, 2022.
30. Layssi, H.; Ghods, P.; Alizadeh, A.R.; Salehi, M. Electrical Resistivity of Concrete. *Concr. Int.* **2015**, *37*, 41–46.
31. Zareei, S.A.; Ameri, F.; Dorostkar, F.; Ahmadi, M. Rice Husk Ash as a Partial Replacement of Cement in High Strength Concrete Containing Micro Silica: Evaluating Durability and Mechanical Properties. *Case Stud. Constr. Mater.* **2017**, *7*, 73–81. [[CrossRef](#)]
32. Adhikary, S.K.; Ashish, D.K.; Rudžionis, Ž. A Review on Sustainable Use of Agricultural Straw and Husk Biomass Ashes: Transitioning towards Low Carbon Economy. *Sci. Total Environ.* **2022**, *838*, 156407. [[CrossRef](#)] [[PubMed](#)]
33. Sahoo, S.; Parhi, P.K.; Chandra Panda, B. Durability Properties of Concrete with Silica Fume and Rice Husk Ash. *Clean. Eng. Technol.* **2021**, *2*, 100067. [[CrossRef](#)]
34. Zunino, F.; Martirena, F.; Scrivener, K. Limestone Calcined Clay Cements (LC3). *ACI Mater. J.* **2021**, *118*, 49–60. [[CrossRef](#)]
35. Yao, W.; Bai, M.; Pang, J.; Liu, T. Performance Degradation and Damage Model of Rice Husk Ash Concrete under Dry–Wet Cycles of Sulfate Environment. *Environ. Sci. Pollut. Res.* **2022**, *29*, 59173–59189. [[CrossRef](#)] [[PubMed](#)]
36. Wu, Z.; Wong, H.S.; Buenfeld, N.R. Transport Properties of Concrete after Drying–Wetting Regimes to Elucidate the Effects of Moisture Content, Hysteresis and Microcracking. *Cem. Concr. Res.* **2017**, *98*, 136–154. [[CrossRef](#)]
37. Sharma, M.; Bishnoi, S.; Martirena, F.; Scrivener, K. Limestone Calcined Clay Cement and Concrete: A State-of-the-Art Review. *Cem. Concr. Res.* **2021**, *149*, 106564. [[CrossRef](#)]
38. Jerman, M.; Scheinherrová, L.; Medved', I.; Krejsová, J.; Doleželová, M.; Bezdička, P.; Černý, R. Effect of Cyclic Wetting and Drying on Microstructure, Composition and Length Changes of Lime-Based Plasters. *Cem. Concr. Compos.* **2019**, *104*, 103411. [[CrossRef](#)]
39. Rahbar, Y.; Mousavi, S.Y.; Nasserabadi, H.D. High-Strength Concrete Containing RHA and Nano-CaCO₃. *Micro Nano Lett.* **2019**, *14*, 1213–1218. [[CrossRef](#)]
40. Maddalena, R.; Taha, H.; Gardner, D. Self-Healing Potential of Supplementary Cementitious Materials in Cement Mortars: Sorptivity and Pore Structure. *Dev. Built Environ.* **2021**, *6*, 100044. [[CrossRef](#)]
41. Cnudde, V.; Cwirzen, A.; Masschaele, B.; Jacobs, P.J.S. Porosity and Microstructure Characterization of Building Stones and Concretes. *Eng. Geol.* **2009**, *103*, 76–83. [[CrossRef](#)]
42. Zajac, M.; Durdzinski, P.; Giergiczny, Z.; Ben Haha, M. New Insights into the Role of Space on the Microstructure and the Development of Strength of Multicomponent Cements. *Cem. Concr. Compos.* **2021**, *121*, 104070. [[CrossRef](#)]
43. Ben Haha, M.; Termkhajornkit, P.; Ouzia, A.; Uppalapati, S.; Huet, B. Low Clinker Systems—Towards a Rational Use of SCMs for Optimal Performance. *Cem. Concr. Res.* **2023**, *174*, 107312. [[CrossRef](#)]
44. Raheem, A.A.; Oriola, K.O.; Kareem, M.A.; Abdulwahab, R. Investigation on Thermal Properties of Rice Husk Ash-Blended Palm Kernel Shell Concrete. *Environ. Chall.* **2021**, *5*, 100284. [[CrossRef](#)]
45. Khushefati, W.H.; Demirboğa, R.; Farhan, K.Z. Assessment of Factors Impacting Thermal Conductivity of Cementitious Composites—A Review. *Clean. Mater.* **2022**, *5*, 100127. [[CrossRef](#)]
46. Ramezani pour, A.A.; Pilvar, A.; Mahdikhani, M.; Moodi, F. Practical Evaluation of Relationship between Concrete Resistivity, Water Penetration, Rapid Chloride Penetration and Compressive Strength. *Constr. Build. Mater.* **2011**, *25*, 2472–2479. [[CrossRef](#)]
47. Avet, F.; Scrivener, K. Investigation of the Calcined Kaolinite Content on the Hydration of Limestone Calcined Clay Cement (LC3). *Cem. Concr. Res.* **2018**, *107*, 124–135. [[CrossRef](#)]
48. Yadak Yaraghi, A.H.; Ramezani pour, A.M.; Ramezani pour, A.A.; Bahman-Zadeh, F.; Zolfagharnasab, A. Evaluation of Test Procedures for Durability and Permeability Assessment of Concretes Containing Calcined Clay. *J. Build. Eng.* **2022**, *58*, 105016. [[CrossRef](#)]
49. Lin, K.L.; Chiang, K.Y.; Lin, C.Y. Hydration Characteristics of Waste Sludge Ash That Is Reused in Eco-Cement Clinkers. *Cem. Concr. Res.* **2005**, *35*, 1074–1081. [[CrossRef](#)]
50. Fuyuan, G.; Dawei, Z.; Evdon, S.; Tamon, U. Empirical Estimation of Pore Size Distribution in Cement, Mortar, and Concrete. *J. Mater. Civil. Eng.* **2014**, *26*, 4014023. [[CrossRef](#)]
51. Ram, K.; Serdar, M.; Londono-Zuluaga, D.; Scrivener, K. The Effect of Pore Microstructure on Strength and Chloride Ingress in Blended Cement Based on Low Kaolin Clay. *Case Stud. Constr. Mater.* **2022**, *17*, e01242. [[CrossRef](#)]
52. Maddalena, R.; Hamilton, A. Low-Pressure Silica Injection for Porosity Reduction in Cementitious Materials. *Constr. Build. Mater.* **2017**, *134*, 610–616. [[CrossRef](#)]

Disclaimer/Publisher's Note: The statements, opinions and data contained in all publications are solely those of the individual author(s) and contributor(s) and not of MDPI and/or the editor(s). MDPI and/or the editor(s) disclaim responsibility for any injury to people or property resulting from any ideas, methods, instructions or products referred to in the content.